Enhancing Irrigation Reservoirs through Floating Photovoltaic: A Satellite Mapping-Based Multifunctional Water-Energy Strategy

Andrés O. Benito[1], Esteban Lannutti[1,2,3] and Pedro Castro Verdezoto[4]

[1] Universidad Tecnológica Nacional, Facultad Regional Mendoza, Mendoza (Argentina)

[2] Instituto Argentino de Nivología, Glaciología y Ciencias Ambientales (IANIGLA), Consejo Nacional de Investigaciones Científicas y Técnicas (CONICET), Mendoza (Argentina)

[3] Universidad Nacional de Cuyo, Facultad de Filosofía y Letra (Argentina)

[4] Universidad de Guayaquil, Facultad de Ingeniería Industrial, Guayaquil (Ecuador)

Abstract

The potential for floating photovoltaics (FPVs) in Mendoza, Argentina, is quantified by mapping irrigation reservoirs with Sentinel-2 imagery and estimating energy yield, water evaporation mitigation, and avoided greenhouse gas (GHG) emissions. A composite Water Index (WI) is developed by linearly combining the NDWI and MNDWI, both derived from Sentinel-2 multispectral satellite imagery. A total of 380 control points (70% calibration, 30% validation) are used to fit WI parameters. Performance is evaluated against MNDWI, AWEIsh, EWI, and a 10-meter deep-learning land-use/land-cover (LULC) map. The new WI achieves the highest accuracy (approximately 98.2%) with the fewest omissions and outperforms all comparators. The application to the Oasis Norte Oeste (ONO) region identifies 524 waterbodies, totaling 5.92 km². After feasibility screening, 3.55 km² (60%) is deemed suitable for FPV deployment. Scenario analysis indicates that covering 10% of the feasible surface would install approximately 6.7 MWp and yield 11,776 MWh per year, scaling up to 60.6 MWp and 117,757 MWh per year at 90% coverage. Avoided GHG emissions are calculated using the CDM ACM0002/TOOL07 methodology, with Argentina's grid factor ranging from 3,415 to 34,150 tCO_2e per year across scenarios. These findings demonstrate that FPV can provide land-neutral electricity generation and substantial climate co-benefits in a water-stressed basin. The WI further offers a robust and transferable workflow for reservoir detection and FPV site screening.

Keywords: Floating Photovoltaics, Multispectral Satellite Imagery, Reservoir mapping, Evaporation mitigation, Renewable Energy, Water Scarcity, Distributed Generation

1. Introduction

Global climate change, rapid population growth, and unsustainable consumption patterns have intensified the global water crisis. Over the past century, water usage has increased sixfold and continues to grow at an annual rate of approximately 1%. Projections indicate that, without significant intervention, the world could experience a water deficit of up to 40% by 2030 (UN & UNESCO, 2020). Water scarcity currently affects approximately four billion people, who experience physical water stress for at least one month each year (Mekonnen et al., 2016). Climate change further exacerbates this issue by intensifying water stress in already vulnerable regions (UNESCO, 2019). Global food security is closely linked to water conservation and availability, as irrigation accounts for about 70% of global freshwater withdrawals, and this figure can reach 90% in developing countries (United Nations, 2024). These interconnected challenges underscore the urgent need to address the complex Water-Energy-Food (WEF) nexus (D'Odorico et al., 2018; Gadzanku et al., 2021).

Simultaneously, global energy demand continues its upward trajectory, projected to increase by almost 50% between 2020 and 2050 under current policy frameworks (EIA, 2023), with agricultural electricity use rising to 26.9% in 2021 (IEA, 2023). To mitigate the effects of climate change and achieve crucial decarbonization goals, such as net zero emissions by 2050, the exponential expansion of renewable energy sources, particularly solar Photovoltaics (PV), is indispensable (Martinez & Iglesias, 2024; Muthia et al., 2024; Ramanan et al., 2024). PV technology has demonstrated robust growth, with capacity increasing by a recorded 18% in 2021 (Delacroix et al., 2023), making it a low-carbon, sustainable, and reliable electricity source (Bassam et al., 2023). Despite these advantages, the extensive land requirements associated with conventional ground-mounted PV (GPV) installations—estimated at around 15,000 m² for a 1 MW PV farm (Amer et al., 2023)

10.18086/swc.2025.06.15 Available at http://proceedings.ises.org

pose significant spatial constraints and create conflict with other productive land uses, such as agriculture (Micheli, 2021; Ghosh, 2023; Bossi, et al., 2024; Exley, et al., 2021).

Mendoza, Argentina, situated within the semi-arid diagonal of South America (Peña et at., 2024; Martín, 2008; Prieto, et al., 2021), exemplifies a region facing severe water scarcity and intense competition for resources. The province, covering 150,839 km², depends almost exclusively on surface water sourced from Andean snowmelt and glacio-nival processes, as the plains receive minimal annual precipitation, typically just over 200 mm. This limited water supply supports the region's three principal oases: Norte, Centro, and Sur. Although these oases comprise only 4% of the province's land area, they accommodate the entire population. Mendoza's economy is predominantly based on agriculture, with the vitiviniculture sector serving as the primary consumptive water user, accounting for approximately 89% of annual water use (Martín, F., 2008) and 71% of Argentina’s total vineyard area (Gobierno de Mendoza, 2024; Instituto Nacional de Vitivinicultura, 2024).

This specialized agro-industrial model has led to significant territorial changes, notably the expansion of the agricultural frontier in the upper Uco Valley within the Central Oasis. This expansion, driven by capital-intensive investments targeting external markets (Mussetta, et al., 2020; Zuniga-Teran, et al., 2021; Prieto, et al., 2021), often relies on groundwater extraction and frequently conflicts with established water management practices. The Uco Valley's distinct hydro-geomorphological characteristics, such as its steep slopes and the lack of a major flow-regulating artificial reservoir, heighten its susceptibility to alluvial events (Mussetta et al., 2020; Zuniga-Teran, et al., 2021). Additionally, water management challenges are intensified by severe and prolonged hydrological droughts, exemplified by the record-setting drought from 2010 to 2015. These environmental pressures, combined with rising urban water demand (Rojas, et al., 2023; Prieto, et al., 2021), require the development of integrated strategies that address both energy provision and water conservation.

Floating photovoltaics (FPV) are increasingly recognized as a multifunctional solution to interconnected energy, water, and land challenges. FPV systems generate low-carbon electricity on underutilized water bodies and offer additional benefits, including reduced evaporation and potential performance improvements through passive cooling and increased albedo (Oliveira-Pinto & Stokkermans, 2020; Gadzanku et al., 2021). Concurrently, the global solar photovoltaic (PV) sector is expanding rapidly, with cumulative capacity reaching approximately 1,185 GW by 2022, which heightens the need to balance energy deployment with competing land uses (Ghosh, 2023). While agrivoltaics represents one approach to land sharing, FPV provides a land-neutral alternative, particularly relevant in land-constrained or water-stressed regions such as Mendoza, Argentina, where extensive irrigation reservoirs exist. FPV is part of the broader category of integrated photovoltaics, which also includes agrivoltaics (Ilgen et al., 2023). Internationally, FPV has advanced from initial pilot projects to multi-megawatt installations, exceeding 2.6 GW of capacity by 2020 across more than 35 countries. The global technical potential is conservatively estimated at approximately 400 GW if 1% of suitable inland water surfaces are utilized (Delacroix et al., 2023; Oliveira-Pinto & Stokkermans, 2020). Despite these developments, FPV remains largely unimplemented in Mendoza and, based on available evidence, throughout Argentina, highlighting a significant opportunity to utilize idle aquatic surfaces such as irrigation reservoirs for clean energy generation and water system benefits.

Floating photovoltaic (FPV) systems deliver coupled water- and energy-system benefits particularly relevant to arid and semi-arid regions (Farra et al., 2022; Abdelal, Q., 2021; Exley et al., 2021). By shading the water surface, FPV can curtail reservoir evaporation—empirical and modeling studies report reductions that can reach tens of percent and, in some contexts, “up to 70%,” with engineering estimates of 7,000–10,000 m³ of water saved per MWp·year in European reservoirs (Garrod et al., 2024). Simultaneously, the over-water microclimate provides passive thermal management for PV modules; multi-site experiments and reviews document lower module temperatures (often 3–10 °C) and energy-yield gains that, while site-dependent, commonly fall in the single-digit range (≈5–7%) and can exceed 10% in favorable conditions (Ghosh, 2023; Cazzaniga et al., 2018). Additional performance contributions may arise from reduced terrestrial dust deposition and the potential for enhanced bifacial irradiance from water reflectance, relative to ground-mounted PV (Garrod et al., 2024). Beyond performance, FPV deployment mitigates land-use conflict by repurposing existing water surfaces for distributed generation (Ramanan et al., 2024). Water-quality responses, however, are nuanced: reduced light can suppress phytoplankton biomass—beneficial for algal-bloom control—yet shading and altered stratification may depress dissolved oxygen and, under certain conditions, favor internal phosphorus release; consequently, design (coverage, spacing) and limnological monitoring are decisive for net outcomes (Rocha et al., 2024; Sibuea et al., 2022). Collectively, these attributes position FPV as a land-neutral complement to ground PV, co-optimizing energy production and water stewardship in water-stressed basins.

This work aimed to develop a tool that quantifies potential renewable energy generation from floating photovoltaic systems in a given area by using satellite detection of agricultural irrigation reservoirs and determining their water surface area, troughtout a novel water extraction index method. The tool also calculates the reduction in water evaporation from these reservoirs because of the area of the solar arrays over free water area and the greenhouse gas (GHG) emissions avoided by replacing grid electricity for agricultural irrigation with power from the floating photovoltaic systems.

2. Materials and Methods

2.1 Water Bodies Mapping

During the waterbody mapping stage, Sentinel-2 multispectral satellite imagery was utilized. The analysis relied on Sentinel-2A and Sentinel-2B Level-1C products, which include radiometric and geometric corrections (Jiang et al., 2021). These products have demonstrated reliable performance for water extraction using various spectral indices. The Normalized Difference Water Index (NDWI) is commonly applied for such purposes. However, delineating waterbodies in urban and mountainous environments presents additional challenges that require more robust indices. NDWI primarily captures vegetation response and may overlook built structures and bare soil, potentially introducing detection errors (Liu et al., 2022).

To address these limitations, the literature frequently employs the Modified Normalized Difference Water Index (MNDWI), which substitutes the near-infrared (NIR) band in NDWI with the shortwave infrared (SWIR) band. Xu (2006) demonstrated that MNDWI identifies waterbodies with greater accuracy. Additional indices, such as the Automated Water Extraction Index–Shadow (AWEIsh) (Feyisa et al., 2014) and the Enhanced Water Index (EWI) (Yan et al., 2007; Wang et al., 2015), have also shown improved results in urban and mountainous settings. These methods combine and weight different indices and spectral bands to enhance extraction under diverse conditions, providing the basis for the current methodology.

Based on this rationale, a composite water index was developed. This index combines and weights NDWI and MNDWI, as defined by the following formula:

$$\mathrm{WI} = a * \frac{\rho\mathrm{Green} - \rho\mathrm{NIR}}{\rho\mathrm{Green} + \rho\mathrm{NIR}} + b * \frac{\rho\mathrm{Green} - \rho\mathrm{SWIR}}{\rho\mathrm{Green} + \rho\mathrm{SWIR}} \qquad \text{(eq. 1)}$$

In this formula, a and b represent calibration parameters, and ρGreen, ρNIR, and ρSWIR denote the reflectances of the green, near-infrared, and shortwave-infrared bands from Sentinel-2 data, respectively. The SWIR band, which has a native spatial resolution of 20 m, was resampled to 10 m using bilinear interpolation to match the spatial resolution of the other bands.

To mitigate seasonal variability in water levels, the Water Index (WI) was calculated by averaging imagery from November 2023 and May 2024. Parameters a and b were then fitted using an automated optimization procedure to minimize the error between WI-based detection and control points. A total of 380 control points were manually digitized, with 190 located over waterbodies and 190 over non-water covers. Of these, 70% (n = 266) were randomly selected for calibration, and 30% (n = 114) were used for validation.

Extraction performance was evaluated by comparing the results of WI, MNDWI, AWEIsh, and EWI against the validation points. For a broader context, the global land-use/land-cover (LULC) map for 2024 developed by Karra et al. (2021) was also included in the comparison. Unlike the spectral indices, this product is derived from a 10-m deep-learning segmentation model trained on more than 5 billion human-labeled Sentinel-2 pixels.

Waterbodies were automatically delineated from the binarized WI using the Moore–Neighbor tracing algorithm (Gonzalez et al., 2004). The resulting polygons were then used to quantify the number and total surface area of available waterbodies in the Oasis Norte Oeste (ONO) region.

2.2 Renewable Power Generation Estimation

In this study, we assume fixed-tilt PV arrays at a 10° inclination, facing geographic north (southern hemisphere), which are nearly horizontal. This common FPV design maximizes power density on limited water footprints, reduces aerodynamic loads, and simplifies mounting and mooring (Trapani et al., 2015; Patil et al., 2017; Friel et al., 2019). While FPV literature reports improved yields due to water-driven cooling and increased albedo, the magnitude is technology and site-dependent. Measured and bankable modeling studies indicate small but positive gains over land arrays (often ≤3%), not the double-digit values sometimes cited anecdotally (Oliveira-Pinto & Stokkermans, 2020).

Annual energy output was calculated using the RETScreen International (2005) model (Eq. 2), developed by Natural Resources Canada (NRC, Ottawa, Canada). The calculation incorporates annual in-plane irradiance, available installation area, conversion efficiencies, temperature derating, and aggregate loss factors.

$$E_A = H_t \times S \times \eta_r \times \eta_{inv} \times \left[1 - \beta_p \times (T_c - 25)\right] \times \left(1 - \lambda_p\right) \times (1 - \lambda_c) \qquad \text{(eq. 2)}$$

Where E_A is annual PV energy (kWh/year) produced by the FPV systems deployed in the surface considered; H_t (kWh/m^2/year) is plane-of-array annual irradiation, which was extracted from the Meteonorm 8.1 database for the geographical center of the study area; S (m^2) is the total area of water bodies detected feasible to install floating solar arrays; η_r (%) is conversion efficiency of the solar cell module; η_{inv} (%) is conversion efficiency of the inverter; β_p (%/°C) is temperature coefficient related to the efficiency of the solar cell module; T_c (°C) is average temperature of the solar cell module, which was estimated from ambient temperature using a standard NOCT-style relationship with an additional FPV cooling term ΔT_{FPV} (°C), (Eq. 3); λ_p (%) is loss coefficient of the solar cell module; and λ_c (%) is loss coefficient of the inverter (Dai et al., 2019; Oliveira-Pinto & Stokkermans, 2020; Ghosh, 2023).

$$T_c \cong T_a + \frac{NOCT - 20}{800} \times G_{POA} - \Delta \mathrm{T}_{FPV} \qquad \text{(eq. 3)}$$

Where T_a (°C) is ambient temperature, NOCT is nominal cell temperature (°C) for a considered Jinko Solar Tiger Neo 66HL5-BDV 715 Watt Bifacial N-type solar panel, and G_{POA} (W/m^2) is clear-sky plane-of-array (POA) irradiance at local solar noon for the central day of each month in Mendoza (lat. −32.89°, long. −68.85°) based on Haurwitz (1945) clear-sky model for Global Horizontal Irradiance (GHI), Erbs (1982) correlation for diffuse fraction, and the isotropic sky transposition Liu & Jordan (1963), for a fixed array tilted 10° and oriented due north (azimuth 0°); the FPV cooling increment ΔT_{FPV} was set as the average value of generally modest consistent temperature drops from published FPV array data (about 0.5 - 3 °C), leading to net energy small but positive gains over ground-mount arrays, as mentioned before. Soiling was set below ground-mount values, reflecting less dust over water, but considered avian droppings risk (Ghosh, 2023).

In this study, the number and surface area of the panels that can be installed in the water bodies detected are calculated, considering module area, spacing requirements and a water bodies FPV feasibility factor, which exclude a minimum buffer to shore and infrastructure, shallow sensitive zones and spacing for O&M walkways and array separation based on wind/wave exposure (Kim, 2019). Then, this result is substituted into equation (2), and finally, the power generation is estimated. Additionally, the power capactity (MW) was obtained taking into account an average energy yield factor for Mendoza's PV systems (Benito et al, 2021), which represents the energy produced per kWp of PV modules installed capacity (System Advisor Model, 2025).

2.3. Water Evaporation Avoided Estimation

Quantifying open-water evaporation is crucial for evaluating the water and energy co-benefits of floating photovoltaic (FPV) systems, as reduced evaporation leads to measurable water savings that can enhance hydropower production, irrigation, and ecological flow regimes (Ghosh, 2023; Ilgen et al., 2023). The classical Penman combination theory requires net radiation, air temperature, humidity, and wind speed to estimate potential evaporation (Penman, 1948). In many reservoirs, wind observations are often unavailable, unrepresentative of over-water conditions, or of uncertain quality. To address this data limitation while retaining the core energy-balance approach, the temperature–radiation formulation developed by Valiantzas (2006) is employed. This method substitutes explicit wind dependence with radiation-normalized and humidity-based terms, while maintaining the structure of the Penman (1948) combination framework.

Potential open-water evaporation (mm per day) is calculated from monthly meteorological data using the simplified expression (eq. 4):

$$E_{PEN} \approx 0.047 R_S \sqrt{T+9.5} - 2.4\left(\frac{R_S}{R_A}\right)^2 + 0.09(T+20)\left(1-\frac{RH}{100}\right) \quad \text{(eq. 4)}$$

In this context, E_{PEN} represents the daily open-water evaporation estimate (mm/d); R_S denotes measured or estimated incoming solar radiation (MJ/m^2/d); T is the mean air temperature for the specified time interval (°C); R_A refers to extraterrestrial solar radiation (MJ/m^2/d) for the site's latitude and Julian day or month; and RH (%) indicates mean relative humidity for the same interval. Extraterrestrial radiation, R_A, and daylight hours, N, are required input parameters required parameters for both the Penman equation and the simplified formula (4). Simplified empirical expressions were used to calculate R_A, and, N for monthly evaporation estimates, following the Valiantzas approach. These simplified formulas provide nearly the same accuracy as the more complex equations of the standardized Penman method, with a relative error of 4% for estimations from Eq. (4).

Monthly evaporation depth $E_{\mathrm{PEN},m}$ (mm/month) (Eq. 5) is multiplied by the effective water surface area A_m (m^2) as determined from the WI index, to yield baseline volumetric losses $V_{\mathrm{base},m}$ (m^3/month):

$$V_{\mathrm{base},m} = \frac{E_{\mathrm{PEN},m}}{1.000} \times A_m \quad \text{(eq. 5)}$$

Time-varying A_m accounts for seasonal shoreline migration and reservoir operation. This geospatial coupling ensures that water-budget terms are consistent with the surface actually available for FPV siting.

2.4. GHG Emissions Reduction

The climate benefit of electricity generated by the FPV portfolio is measured using a consequential accounting approach. In this method, avoided grid emissions are determined by multiplying the annual FPV electricity supplied to the grid by a grid-specific Argentine emission factor (tCO_2e per MWh) (Eq. 6). Avoided emissions are calculated as follows:

$$GHG_{CO_{eq_{Avoided}}} = f_{CO_{eq_{PVEE}}} \times EN_{EEFPV} \quad \text{(eq. 6)}$$

Where $GHG_{CO_{eq_{Avoided}}}$ (tCO_{2eq}/year) denotes the total greenhouse gas emissions (GHG) avoided by the system; $f_{CO_{eq_{PVEE}}}$ (tCO_{2eq}/MWh) s the characterization factor for electrical energy generated from feasible FPV deployment at varying percentages of water surface coverage; and EN_{EEFPV} (MWh/year) represents the substituted energy from the Argentine energy matrix.

We use the ex-post simple operating margin factor, which underlies official estimates of emission reductions. This follows Clean Development Mechanism (CDM) (UNFCCC, 2022) methodology *ACM0002* (UNFCCC, 2022) and TOOL07 (tool to calculate the emission factor for an electricity system) (UNFCCC, 2018). The National Inventory Report, in its First Biennial Transparency Report of the Argentine Republic to the United

Nations Framework Convention on Climate Change (IBT1) calculates annual renewable policy reductions as net renewable generation times the ex-post operating margin factor (SSAmb., 2024). CH_4 and N_2O are excluded because their impact is negligible for the grid. The size of this factor is supported by Argentina's National Inventory which gives a national-average grid emission factor of 0.29 tCO_2/MWh for 2022. This uses total electricity emissions and annual generation data from CAMMESA (MAyDS, 2024). This average serves as a conservative fallback when detailed operating margin values are unavailable.

3. RESULTS AND DISCUSSION

Figure 1 shows the location of the North-West Oasis (ONO) and the control points used for calibration and validation. The optimization procedure fitted the Water Index (WI) with parameters a = 2.50 and b = 0.28, resulting in 98.4% accuracy during calibration. This accuracy corresponds to correctly classifying approximately 49 out of every 50 water features, including ponds and irrigation bodies. Using a threshold of 0.3, the method produced three false negatives (missed waterbodies) and one false positive (incorrect water detection) out of 266 points. The threshold indicates the WI value above which a pixel is classified as water.

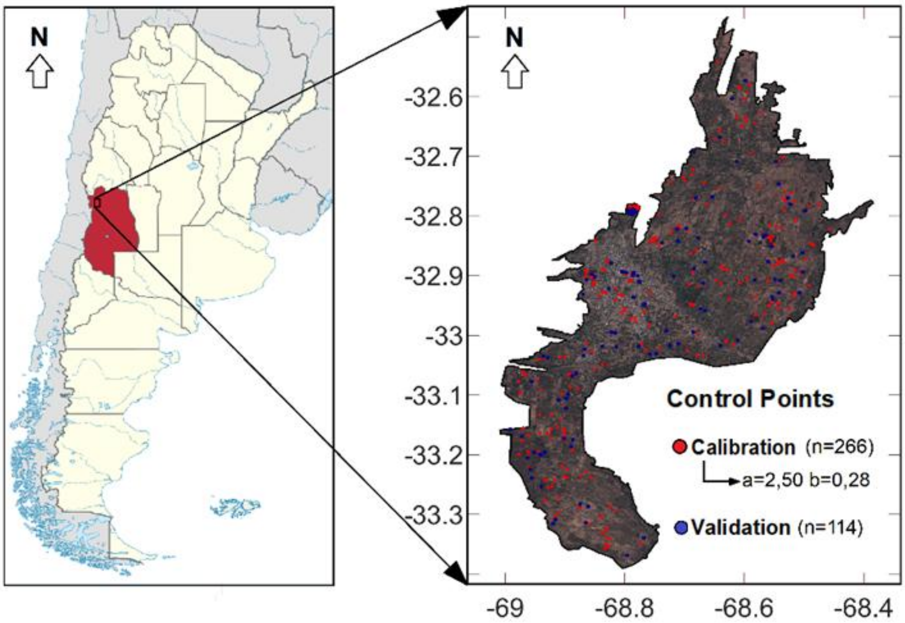

Figure 1. Location of the ONO and distribution of digitized control points.

The Water Index (WI) developed in this study achieved the highest overall accuracy and the fewest false negatives among the evaluated methods. Table 1 provides a comparative summary of WI, Modified Normalized Difference Water Index (MNDWI), Automated Water Extraction Index for shadow (AWEIsh), Enhanced Water Index (EWI), and Land Use/Land Cover (LULC) classification against the validation points. The table reports commission errors (false positives), omission errors (false negatives), and overall accuracy for each method. LULC showed the lowest accuracy and frequently failed to detect water pixels. AWEIsh produced the most false positives among the spectral indices. MNDWI and EWI demonstrated a more balanced performance between false positives and false negatives, with EWI achieving higher accuracy than MNDWI. The WI proposed in this study outperformed all other methods, achieving the highest overall accuracy and only two false negatives.

Figure 2 displays the mapped waterbodies within the North-West Oasis (ONO) region, generated using the proposed Water Index (WI). The color scale indicates that higher WI values correspond to a greater probability of water presence. Panels A and B show enlarged views of two areas containing waterbodies, highlighting the spatial detail achieved. Figure 3 illustrates two zones with examples of polygons extracted after binarizing the WI at a threshold of 0.3 and applying the contour-tracing algorithm. These examples demonstrate that the WI accurately identified waterbodies in challenging environments such as croplands, built-up areas, and anti-hail netting, where satellite multispectral methods often produce false positives.

Table 1: Summary of performance achieved by the WI, MNDWI, AWEIsh, EWI, and LULC indices against validation points.

Index	False positives	False negatives	Accuracy (%)
WI	0	2	98,2
MNDWI	2	7	92,1
AWEIsh	10	0	91,2
EWI	2	1	97,4
LULC	0	20	82,5

The application of the WI method resulted in the detection of 524 waterbodies, with a mean surface area of 11,303 m² and a total surface area of 5,922,800 m² (5.92 km²).

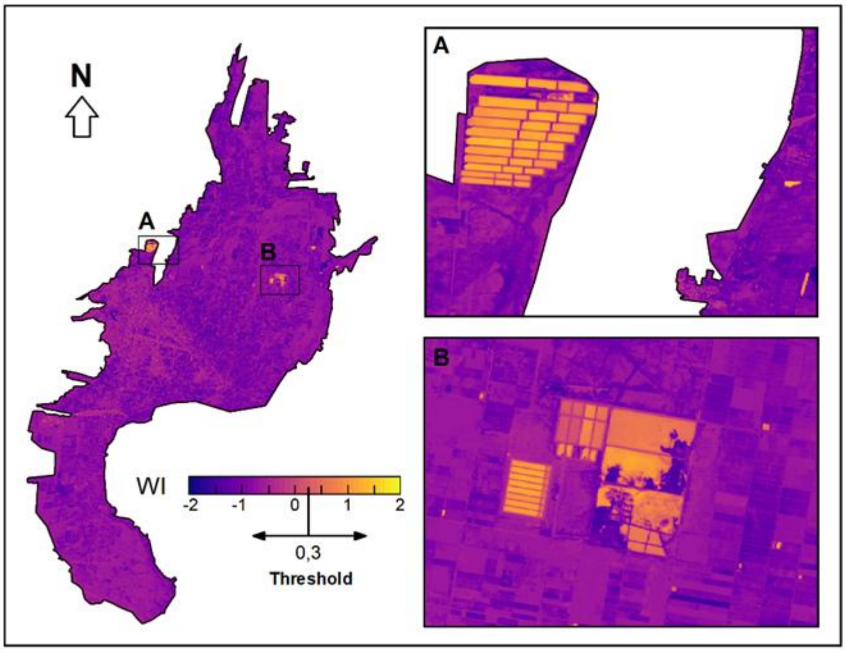

Figure 2. Waterbody mapping generated with the WI in the ONO region.

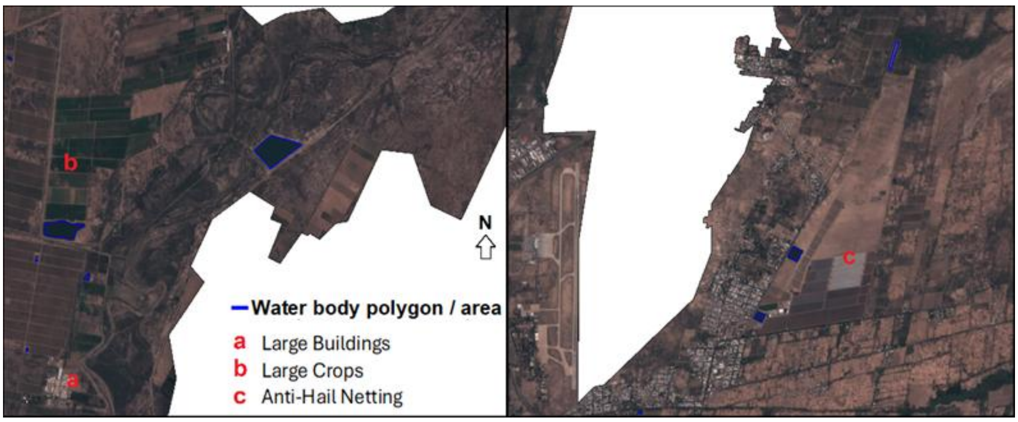

Figure 3. Examples of polygons corresponding to waterbodies derived from the WI.

The floating photovoltaic (FPV) capacity and power production for the detected water bodies were calculated using a 60% FPV feasibility factor, resulting in a total feasible water area of 3,553,680 m². The calculations considered solar irradiance, PV module characteristics, inverter specifications, and various FPV system area-to-water area ratios. An additional 11% efficiency was included for floating PV systems (Jeong et al., 2020).

Table 2 presents the results of this analysis. Installing FPV panels on 10% of the feasible water area yields a total installed capacity of approximately 6.7 MWp and an annual power generation of 11,776 MWh. In recent years, floating PV has been installed on a high percentage of reservoir areas in several cases (Nobre, 2025). If FPV systems are installed on 90% of the feasible water area, the total installed capacity is estimated at 67.3 MWp, with an annual power production of 117,757 MWh.

The water evaporation avoided from the entire feasible water bodies area was estimated for various ratios of surface coverage by FPV structures. The range extends from 8.34×10^6 m^3/year for 10% coverage to 9.2×10^6 m^3/year for 90% coverage. Implementing FPV systems over water bodies could result in water savings of up to 787.2 m^3/MWh, equivalent to 1.37×10^6 m^3/MWp/year. These results are presented in Table 2.

Greenhouse gas (GHG) emissions avoided from the entire feasible water bodies area were estimated for different ratios of surface coverage by FPV systems. At 10% coverage, 3,415 tCO2eq/year would be avoided, while 90% coverage would result in 34,150 tCO2eq/year avoided.

Table 2: The results of floating photovoltaic system installations according to the ratio of the installation area over the total feasible area of water bodies detected.

FPV System Area to Reservoir Area Ratio (%)	**10**	**20**	**30**	**40**	**50**	**90**
Annual Power Generation (MWh/year)	11,776	23,551	35,327	47,103	58,879	117,757
Power Capacity of FVP (MW)	6.7	13.5	20.2	26.9	33.6	60,6
Water Evaporation Avoided (MM m^3/year)	83.4	74.1	64.8	55.6	46.3	83.4
Greenhouse Gas Emissions Avoided (tCO_{2eq}/year)	3,415	6,830	10,245	13,660	17,075	26,247

4. CONCLUSIONS

Floating Photovoltaic (FPV) technology represents a promising and strategic approach to addressing global challenges related to the Water-Energy-Food (WEF) nexus, particularly in areas experiencing water scarcity and irrigation stress. This technology demonstrates documented technical advantages compared to conventional ground-mounted photovoltaic systems.

A primary advantage identified in the literature is increased energy production efficiency. The cooling effect of the underlying water reduces the operating temperature of photovoltaic modules, typically resulting in higher efficiency and yield compared to terrestrial systems. Additionally, FPV systems experience less soiling and fewer shading obstacles.

From a resource management perspective, FPV systems play a significant role in water conservation by reducing evaporation from water surfaces, which is particularly beneficial in arid and semi-arid regions. This reduction in evaporation directly supports regional water security. Additionally, FPV deployment minimizes land use, thereby avoiding competition with agricultural or urban development. Integration with existing hydroelectric power plants can enhance energy system stability and increase renewable energy output by utilizing established grid infrastructure. Although FPV currently requires higher initial capital expenditure (CAPEX), anticipated cost reductions from technological advancements and economies of scale are expected to improve profitability.

Despite these advantages, the rapid deployment of FPV technology has outpaced the foundational understanding of its long-term interactions with aquatic environments. This gap in ecological knowledge constitutes a significant challenge for sustainable future expansion.

To support the sustainable expansion and optimal performance of FPV technology, future research should address several critical areas. First, integrated environmental and ecological assessment requires comprehensive, long-term empirical studies to systematically quantify the physical, chemical, and biological impacts of FPV systems on water bodies, including effects on water quality and aquatic ecosystems. Standardized monitoring approaches are necessary to accurately evaluate cascading ecological effects. Second, technological development and system optimization should focus on advancing FPV configurations, such as tracking mechanisms, bifacial modules, and hybrid systems. The development of dedicated numerical modeling software is also required to accurately predict FPV performance, as current commercial tools often need significant adaptation. Third, economic and policy frameworks must be strengthened through detailed techno-economic analyses that quantify the financial value of benefits such as water savings and avoided carbon dioxide emissions relative to total lifetime costs. Establishing standard guidelines and best practices is also crucial for reducing investment risk and ensuring regulatory compliance.

This study demonstrates that integrating a composite Water Index derived from Sentinel-2 imagery with a geospatial and technoeconomic analysis pipeline establishes a transparent and transferable framework for early-stage floating photovoltaic (FPV) site screening. The Water Index, formulated as a linear combination of the Normalized Difference Water Index (NDWI) and the Modified NDWI (MNDWI), effectively delineates irrigation reservoirs. The pipeline quantifies FPV capacity, annual energy generation, evaporation reduction, and greenhouse gas (GHG) abatement. When applied to the North-West Oasis (ONO), this integrated methodology produces internally consistent, decision-relevant metrics that identify significant siting opportunities with minimal land-use conflict. The findings suggest that ONO possesses considerable practical potential for FPV development. Furthermore, the combined approach is readily scalable to other basins in Mendoza and throughout Argentina.

5. REFERENCES

World Water Development Report 2020: Water and Climate Change, 2020. UNESCO. https://www.unesco.org/en/articles/world-water-development-report-2020-water-and-climate-change

Mekonnen, M.M., Hoekstra & A.Y. (2016). Four billion people facing severe water scarcity. Science Advances 2. https://doi.org/10.1126/sciadv.1500323

UN & UNESCO. Agua y Cambio Climático. Cuarto informe mundial de las Naciones Unidas sobre el desarrollo de los recursos hídricos. Programa mundial de evaluación de los recursos hídricos, 2020.

WWAP (UNESCO World Water Assessment Programme). 2019. The United Nations World Water Development Report 2019: Leaving No One Behind. Paris, UNESCO.

United Nations, The United Nations World Water Development Report 2024: Water for Prosperity and Peace. UNESCO, Paris.

D'Odorico, Davis, P., Rosa, K. F., Carr, L., Chiarelli, J. A., Dell'Angelo, D., Gephart, J., MacDonald, J., Seekell, G. K., Suweis, D., Rulli, S. & Cristina, M. (2018). The Global Food-Energy-Water Nexus. Reviews of Geophysics 56. https://doi.org/10.1029/2017RG000591

Gadzanku, S.; Mirletz, H.; Lee, N.; Daw, J.; Warren, A. Benefits and Critical Knowledge Gaps in Determining the Role of Floating Photovoltaics in the Energy-Water-Food Nexus. Sustainability 2021, 13, 4317. https://doi.org/10.3390/su13084317

U.S. Energy Information Administration, International Energy Outlook 2023 (IEO2023)

International Energy Agency, "World Energy Balances 2021: Extended Energy Balances", August 2023, https://www.iea.org/data-and-statistics/data-product/world-energy-balances.

Martinez, A., & Iglesias, G. (2024). Floating solar photovoltaics in the Mediterranean Sea: Mapping and sensitivity analysis of the levelised cost of energy. Journal of Cleaner Production, 473, 143534.

Muthia, R., Pramudya, A. S. P., Maulana, M. R., & Purwanto, W. W. (2024). Techno–economic analysis of green hydrogen production by a floating solar photovoltaic system for industrial decarbonization. Clean Energy, 8(4), 1-14.

Ramanan, C. J., Lim, K. H., Kurnia, J. C., Roy, S., Bora, B. J., & Medhi, B. J. (2024). Towards sustainable power generation: Recent advancements in floating photovoltaic technologies. Renewable and Sustainable

Energy Reviews, 194, 114322.

Delacroix, S., Bourdier, S., Soulard, T., Elzaabalawy, H., & Vasilenko, P. (2023). Experimental modelling of a floating solar power plant array under wave forcing. Energies, 16(13), 5198.

Bassam, A. M., Amin, I., Mohamed, A., Elminshawy, N. A., Soliman, H. Y., Elhenawy, Y., ... & Oterkus, E. (2023). Conceptual design of a novel partially floating photovoltaic integrated with smart energy storage and management system for Egyptian North Lakes. Ocean Engineering, 279, 114416.

Amer, A., Attar, H., As'ad, S., Alsaqoor, S., Colak, I., Alahmer, A., Alali, M., Borowski, G., Hmada, M. & Solyman, A. (2023). Floating Photovoltaics: Assessing the Potential, Advantages, and Challenges of Harnessing Solar Energy on Water Bodies. Journal of Ecological Engineering, 24(10), 324–339. https://doi.org/10.12911/22998993/170917

Micheli, L. (2021). Energy and economic assessment of floating photovoltaics in Spanish reservoirs: cost competitiveness and the role of temperature. Solar Energy, 227, 625-634.

Ghosh, A. (2023). A comprehensive review of water based PV: Flotavoltaics, under water, offshore & canal top. Ocean Engineering, 281, 115044.

Bossi, S., Blasi, L., Cupertino, G., dell'Erba, R., Cipollini, A., De Vito, S., Santoro, M., Di Francia, G., & Tina, G. M. (2024). Floating Photovoltaic Plant Monitoring: A Review of Requirements and Feasible Technologies. Sustainability, 16(19), 8367. https://doi.org/10.3390/su16198367

Exley, G., Hernandez, R. R., Page, T., Chipps, M., Gambro, S., Hersey, M., ... & Armstrong, A. (2021). Scientific and stakeholder evidence-based assessment: Ecosystem response to floating solar photovoltaics and implications for sustainability. Renewable and Sustainable Energy Reviews, 152, 111639.

Peña, N. E., Martin, L., Ocampo, R. S., D'Inca, V., Razquin, O., Sánchez, J. B., & Andino, M. (2024). Planificación territorial urbana y gestión integrada de cuencas en perspectiva comparada. Los ríos Mendoza (Argentina) y Aconcagua (Chile). Revista Geográfica de Chile Terra Australis, 60(1).

Martín, F. (2008). Agua y modelo productivo. Innovaciones tecnológicas e impactos territoriales en el sistema agroalimentario de Mendoza. Estudios socioterritoriales. Revista de geografía, (7), 26-45.

Prieto, M. D. R., Rojas, J. F., Martin, F. D., Araneo, D. C., Villalba, R., Rivera, J. A., & Gil Guirado, S. (2024). Sequías extremas en Mendoza durante el siglo XX y principios del XXI: Administración de la carencia y conflictos socio-políticos.

Gobierno de Mendoza, Subsecretaría de Comunicación Social, Prensa y Protocolo. (2024). Dossier económico: Vendimia 2024. Gobierno de Mendoza.

Instituto Nacional de Vitivinicultura. (2024, February). Informe anual de superficie 2023 (Base de datos congelada al 31/12/23). http://www.inv.gob.ar/ (accesed August 2025).

Mussetta, P., Parise Schneider, N., & Ivars, J. (2020). Produciendo el oasis, transfiriendo vulnerabilidades. Particularidades hidro-geomorfológicas y transformaciones socio productivas en el Valle de Uco, Mendoza, Argentina. Revista de Geografía Norte Grande, (75), 131-151.

Zuniga-Teran, A. A., Mussetta, P. C., Ley, A. N. L., Díaz-Caravantes, R. E., & Gerlak, A. K. (2021). Analyzing water policy impacts on vulnerability: Cases across the rural-urban continuum in the arid Americas. Environmental Development, 38, 100552.

Rojas, F., Sironi, O., & Martín, F. (2023). Sequías en Mendoza (Argentina): una mirada sociohistórica desde la segunda mitad del siglo XIX. Agua y territorio= Water and Landscape, (22), 147-166.

Oliveira-Pinto, S., & Stokkermans, J. (2020). Assessment of the potential of different floating solar technologies–Overview and analysis of different case studies. Energy conversion and Management, 211, 112747.

Gadzanku, S., Mirletz, H., Lee, N., Daw, J., & Warren, A. (2021). Benefits and critical knowledge gaps in determining the role of floating photovoltaics in the energy-water-food nexus. Sustainability, 13(8), 4317.

Ghosh, A. (2023). A comprehensive review of water based PV: Flotavoltaics, under water, offshore & canal top. Ocean Engineering, 281, 115044.

Ilgen, K., Schindler, D., Wieland, S., & Lange, J. (2023). The impact of floating photovoltaic power plants on lake water temperature and stratification. scientific reports, 13(1), 7932.

Delacroix, S., Bourdier, S., Soulard, T., Elzaabalawy, H., & Vasilenko, P. (2023). Experimental modelling of a floating solar power plant array under wave forcing. Energies, 16(13), 5198.

Farrar, L. W., Bahaj, A. S., James, P., Anwar, A., & Amdar, N. (2022). Floating solar PV to reduce water evaporation in water stressed regions and powering water pumping: Case study Jordan. Energy Conversion and Management, 260, 115598.

Abdelal, Q. (2021). Floating PV; an assessment of water quality and evaporation reduction in semi-arid regions. International Journal of Low-Carbon Technologies, 16(3), 732-739.

Exley, G., Hernandez, R. R., Page, T., Chipps, M., Gambro, S., Hersey, M., ... & Armstrong, A. (2021). Scientific and stakeholder evidence-based assessment: Ecosystem response to floating solar photovoltaics and implications for sustainability. Renewable and Sustainable Energy Reviews, 152, 111639.

Garrod, A., Hussain, S. N., Ghosh, A., Nahata, S., Wynne, C., & Paver, S. (2024). An assessment of floating photovoltaic systems and energy storage methods: A comprehensive review. Results in Engineering, 21, 101940.

Cazzaniga, R., Cicu, M., Rosa-Clot, M., Rosa-Clot, P., Tina, G. M., & Ventura, C. (2018). Floating photovoltaic plants: Performance analysis and design solutions. Renewable and Sustainable Energy Reviews, 81, 1730-1741.

Ramanan, C. J., Lim, K. H., Kurnia, J. C., Roy, S., Bora, B. J., & Medhi, B. J. (2024). Towards sustainable power generation: Recent advancements in floating photovoltaic technologies. Renewable and Sustainable Energy Reviews, 194, 114322.

Rocha, S. M., Armstrong, A., Thackeray, S. J., Hernandez, R. R., & Folkard, A. M. (2024). Environmental impacts of floating solar panels on freshwater systems and their techno-ecological synergies. Environmental Research: Infrastructure and Sustainability, 4(4), 042002.

Sibuea, R. T., Pratna, R., Hapsari, A., & Kristi, Y. W. (2022, April). Satellite remote sensing using earth observing system in environmental monitoring for hydropower & floating photovoltaic reservoir (case study: Algae blooming on cirata reservoir, west java-Indonesia). In IOP conference series: earth and environmental science (Vol. 1009, No. 1, p. 012001). IOP Publishing.

Jiang, H., Wang, M., Hu, H., & Xu, J. (2021). Evaluating the performance of Sentinel-1A and Sentinel-2 in small waterbody mapping over urban and mountainous regions. Water, 13(7), 945.

Liu, H., Hu, H., Liu, X., Jiang, H., Liu, W., & Yin, X. (2022). A comparison of different water indices and band downscaling methods for water bodies mapping from Sentinel-2 imagery at 10-M resolution. Water, 14(17), 2696.

Xu, H. (2006). Modification of normalised difference water index (NDWI) to enhance open water features in remotely sensed imagery. International journal of remote sensing, 27(14), 3025-3033.

Feyisa, G.L.; Meilby, H.; Fensholt, R.; Proud, S.R. Automated Water Extraction Index: A new technique for surface water mapping using Landsat imagery. Remote Sens. Environ. 2013, 140, 23–35.

Yan, Y., Y. Zhang, and Y. Zhang. 2007. "Study on Extraction of Water System Information in Semi-arid Regions Using Enhanced Water Body Index (EWI) and GIS Denoising Technology (in Chinese)." Remote Sensing Information 06: 62–67.

Wang, S., Baig, M. H. A., Zhang, L., Jiang, H., Ji, Y., Zhao, H., & Tian, J. (2015). A simple enhanced water index (EWI) for percent surface water estimation using Landsat data. IEEE Journal of Selected Topics in Applied Earth Observations and Remote Sensing, 8(1), 90-97.

Karra, K., Kontgis, C., Statman-Weil, Z., Mazzariello, J. C., Mathis, M., & Brumby, S. P. (2021, July). Global land use/land cover with Sentinel 2 and deep learning. In 2021 IEEE international geoscience and remote sensing symposium IGARSS (pp. 4704-4707). IEEE.

Gonzalez, R. C., Woods, R. E., & Eddins, S. L. (2004). Digital image processing using MATLAB. Pearson Education India.

Friel, D., Karimirad, M., Whittaker, T., Doran, W. J., & Howlin, E. (2019, October). A review of floating photovoltaic design concepts and installed variations. In 4th International Conference on Offshore Renewable Energy. CORE2019 proceedings, Glasgow: ASRANet Ltd, UK, 30 Aug 2019. ASRANet Ltd.

Trapani, K., & Redón Santafé, M. (2015). A review of floating photovoltaic installations: 2007–2013. Progress in Photovoltaics: Research and Applications, 23(4), 524-532.

Patil Desai Sujay, S., Wagh, M. M., & Shinde, N. N. (2017). A review on floating solar photovoltaic power plants. Int. J. Sci. Eng. Res, 8, 789-794.

RETScreen International Clean Energy Decision Support Centre. Clean Energy Project Analysis, RETScreen Engineering & Cases Textbook; CANMET Energy Technology Centre: Montreal, QC, Canada, 2005.

Haurwitz, B. (1945). Insolation in relation to cloudiness and cloud density. Journal of Meteorology, 2(3), 154–166.

Erbs, D. G., Klein, S. A., & Duffie, J. A. (1982). Estimation of the diffuse radiation fraction for hourly, daily and monthly-average global radiation. Solar Energy, 28(4), 293–302.

Liu, B. Y. H., & Jordan, R. C. (1963). The long-term average performance of flat-plate solar-energy collectors. Solar Energy, 7(2), 53–74.

Dai, J., Zhang, C., Lim, H. V., Ang, K. K., Qian, X., Wong, J. L. H., ... & Wang, C. L. (2020). Design and construction of floating modular photovoltaic system for water reservoirs. Energy, 191, 116549.

Kim, S. M., Oh, M., & Park, H. D. (2019). Analysis and prioritization of the floating photovoltaic system potential for reservoirs in Korea. Applied Sciences, 9(3), 395. DOI:10.3390/app9030395.

System Advisor Model™ Version 2025.4.16 (SAM™ 2025.4.16) User Documentation. Weather File Formats. National Renewable Energy Laboratory. Golden, CO.

Benito, A. O., López, M. L., Henderson, G., Arena, A. P., Burlot, A., & Filice, J. M. (2021). Análisis de desempeño técnico-económico de sistema fotovoltaico en integración edilicia: Caso edificio Nave Cultural de Mendoza. En Reunión de Trabajo de la Asociación Argentina de Energías Renovables y Medio Ambiente (ASADES 2021). Asociación Argentina de Energías Renovables y Medio Ambiente (ASADES).

Valiantzas, J. D. (2006). Simplified versions for the Penman evaporation equation using routine weather data. Journal of Hydrology, 331(3-4), 690-702.

Penman, H.L., 1948. Natural evaporation from open water, bare and grass. Proc. R Soc. Lond. Ser. A 193, 120–145.

United Nations Framework Convention on Climate Change (UNFCCC). (2022, December). CDM Methodology Booklet (up to EB 116). UNFCCC. https://cdm.unfccc.int/

UNFCCC. (2022, July 13). ACM0002: Grid-connected electricity generation from renewable sources (Version 21.0). UNFCCC/CDM. https://cdm.unfccc.int/

UNFCCC. (2018, August 31). Tool to calculate the emission factor for an electricity system (TOOL07) (Version 07.0). UNFCCC/CDM. https://cdm.unfccc.int/

SSAmb. 2024. Primer Informe Bienal de Transparencia (IBT1) de la República Argentina a la Convención Marco de las Naciones Unidas sobre el Cambio Climático (CMNUCC).

Jeong, H. S., Choi, J., Lee, H. H., & Jo, H. S. (2020). A study on the power generation prediction model considering environmental characteristics of floating photovoltaic system. Applied Sciences, 10(13), 4526.

Nobre, R. L., Vagnon, C., Boulêtreau, S., Colas, F., Azémar, F., Tudesque, L., ... & Cucherousset, J. (2025). Floating photovoltaics strongly reduce water temperature: A whole-lake experiment. Journal of Environmental Management, 375, 124230.